



Comparison of snow water equivalent retrieved from SSM/I passive microwave data using artificial neural network, projection pursuit and nonlinear regressions

Thian Yew Gan ^{a,*}, Oscar Kalinga ^b, Purushottam Singh ^c

^a Department of Civil and Environmental Engineering, University of Alberta, Edmonton, Alberta, Canada T6G 2W2

^b Golder Associates Ltd., Calgary, Alberta, Canada

^c Golder Associates Ltd., Suite 202-2790, Gladwin Road, Abbotsford, BC, Canada V2T 4S8

ARTICLE INFO

Article history:

Received 22 May 2008

Received in revised form 5 January 2009

Accepted 11 January 2009

Keywords:

SSM/I passive microwave data

Brightness temperature

Snow water equivalent

Artificial neural network

Statistical regression models

ABSTRACT

The snow water equivalent (SWE) for the Red River basin of North Dakota and Minnesota was retrieved from data acquired by passive microwave SSM/I (Special Sensor Microwave Imager) sensors mounted on the US Defense Meteorological Satellite Program (DMSP) satellites, physiographic and atmospheric data by an artificial neural network called Modified Counter Propagation Network (MCPN), a Projection Pursuit Regression (PPR) and a nonlinear regression. The airborne gamma-ray measurements of SWE for 1989 and 1997 were used as observed SWE, and SSM/I data of 19 and 37 GHz frequencies, in both horizontal and vertical polarization, were used for the calibration (1989 data from DMSP-F8) and validation (1997 data from DMSP-F10 and F13 of both ascending and descending overpass times were combined) of the models. The SSM/I data were screened for the presence of wet snow, large water bodies like lakes and rivers, and depth-hoar. The MCPN model produced encouraging results in both calibration and validation stages (R^2 was about 0.9 for both calibration (C) and validation (V)), better than PPR (R^2 was 0.86 for C and 0.62 for V), which in turn was better than the multivariate nonlinear regression at the calibration stage (R^2 was 0.78 for C and 0.71 for V). MCPN is probably better than the linear and nonlinear regression counterparts because of its parallel computing structure resulted from neurons interconnected by a parallel network and its ability to learn and generalize information from complex relationships such as the SWE-SSM/I or other relationships encountered in geosciences.

© 2009 Elsevier Inc. All rights reserved.

1. Introduction

Snow is the major source of fresh water for municipal and industrial water supply, irrigation, and hydropower generation over wide regions of the mid-latitude covered by the snow for a large part of the year (Shi & Dozier, 2000). For example, in the Canadian Prairies, as much as 80% of the annual surface runoff is generated from snow cover, and snowfall accounts for up to 90% of the annual water supply in the Colorado Rockies and Sierra Nevada of California. It is therefore important to gather accurate information on the spatial and temporal variation of snow parameters such as area cover, snow depth and snow water equivalent (SWE), which is the amount of water in a snowpack after complete melting.

Owing to the huge cost in collecting ground measurements of snow, and the harsh environment in remote areas such as mountains dominated by snowpack, the ground observation of snowpack data is usually very sparse or not available at all. Therefore, practically the only feasible alternative for collecting comprehensive snowpack information on a regional basis is through remote sensing, i.e.

airborne and space borne data, and in our study the airborne snow measurements were conducted by the Radiation Survey Program of National Weather Service (NWS) of USA using a gamma-ray spectrometer (NWS, 1992). The Office of Hydrology of NWS has been measuring SWE using airborne gamma radiation with as many as 1578 flight lines in 32 states/provinces of the United States. Airborne gamma radiation acquired at some transects were calibrated against field observed SWE to establish the retrieval algorithms for such airborne data. Recently remotely sensed snowpack data have been used for climate related studies (e.g., Dyer & Mote, 2007; Sobolowski & Frei, 2007).

The launching of passive microwave remote sensing sensors e.g., the Scanning Multichannel Microwave Radiometer (SMMR) prior to 1987 and the Special Sensor Microwave Imager (SSM/I) after 1987, and in recent years, the Advanced Microwave Scanning Radiometer-EOS (AMSR-E) (Armstrong et al., 2003) has played important roles in the snow research, and various snow retrieval algorithms have been developed and applied (e.g., Chang et al., 1982; Ferraro et al., 1994; Gan, 1996; Goodison, 1989; Hallikainen & Jolma, 1992; Mekis & Hopkinson, 2004; Singh & Gan, 2000; Walker & Goodison, 1993; Wilson et al., 1999). The dense media radiative transfer theory has also been used to apply passive microwave data in snow mapping (Tsang

* Corresponding author. Tel.: +1 780 492 9376.

E-mail address: tgan@ualberta.ca (T.Y. Gan).

et al., 2000). Recently, there have been snow studies conducted using data of MODIS (Moderate Resolution Imaging Spectroradiometer) sensor on board Terra (since 2000) and Aqua satellites (since 2002) (e.g., Hall et al., 2002; Salomonson & Appel, 2006; Tekeli et al., 2005). However, data from optical sensors such as MODIS can only be used to retrieve snow cover and albedo. In applying SSM/I data for retrieving SWE, often brightness temperatures (TB) of both vertical and

horizontal polarizations at 19 and 37 GHz (V19, H19, V37, and H37) are used (Chen et al., 2001). Different algorithms use different combination of these TB, together with physiographic and climate data in some cases, to retrieve snow data, particularly SWE.

The physical basis of microwave detection of snow lies in the snow scattering property of incident microwave radiation, which depends on the snow grain size, snow density, depth, snow water equivalent,

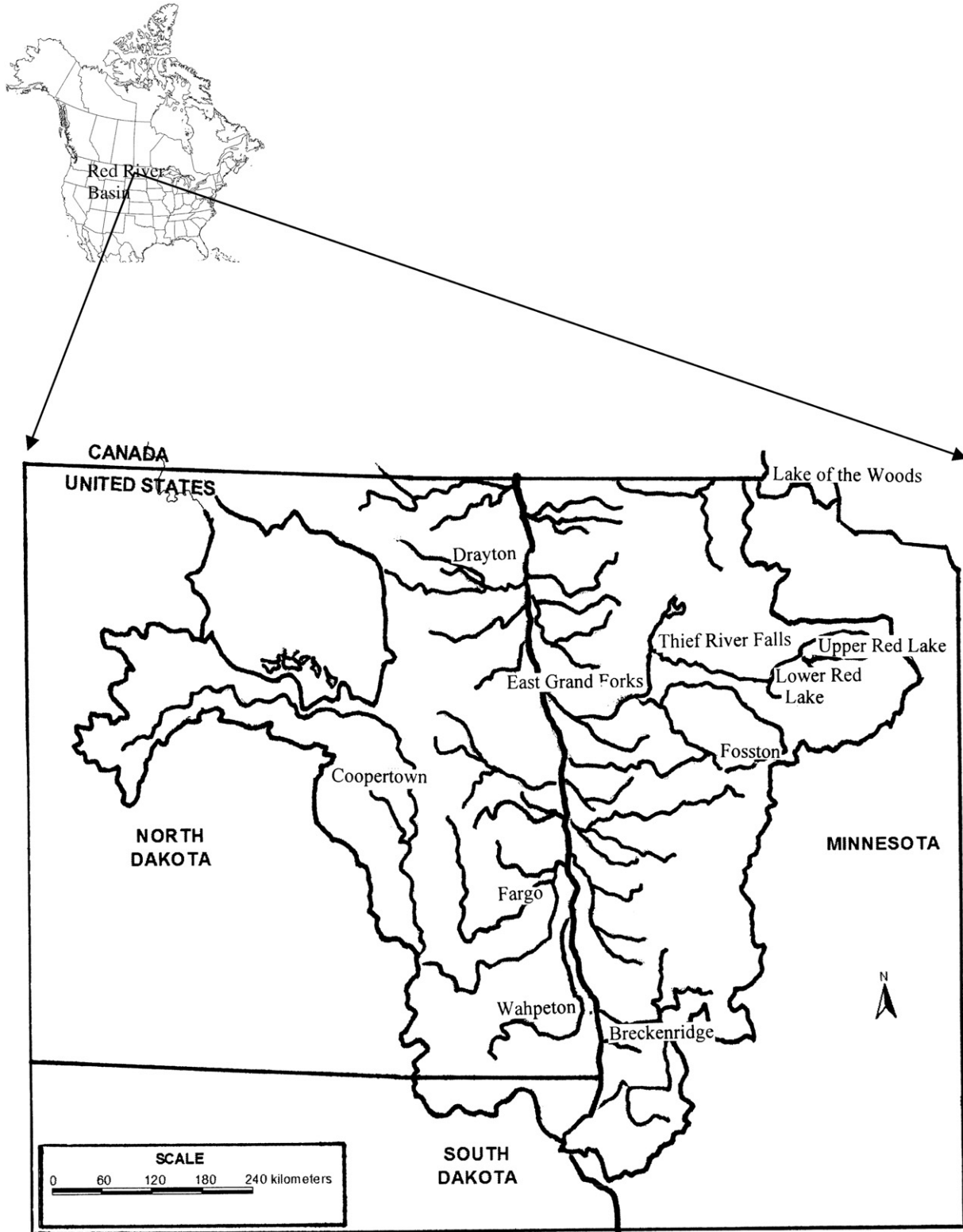


Fig. 1. The Red River basin of Eastern North Dakota and northwestern Minnesota.

Table 1

SSM/I data from DMSP satellites and SWE Estimated from Airborne Gamma-Ray Data with data satisfying the dry snow criteria shown in square brackets.

Year	Satellite data source and projection	Total airborne data	Total gridded airborne data	Maximum SWE (cm)	Minimum SWE(cm)	Mean (cm)	Standard deviation (cm)
1988	DMSP F8 NSIDC EASE-Grid	65	52 [13]	11.80 [6.95]	0.00 [0.60]	3.49 [3.42]	2.73 [2.12]
1989	DMSP F8 NSIDC EASE-Grid	241	175 [121]	15.70 [15.65]	3.30 [4.60]	9.29 [9.24]	2.43 [2.17]
1997	DMSP F10 and F13 MSFC, Swath Data	192	197 [117]	21.80 [19.40]	1.00 [7.20]	12.44 [13.50]	4.02 [3.02]

[] Dry snow cases based on four criteria ($V37 < 250^\circ\text{K}$; $V19 - V37 = > 9^\circ\text{K}$; $V37 - H37 = > 10^\circ\text{K}$; and $p\text{-factor} > 0.026$).

temperature, degree of metamorphism, nocturnal crust development, ice lenses and others (Mätzler, 1994). For instance, theoretically the greater the depth of snow, the lower should be the SSM/I TB if other climatic and snowpack conditions remain the same, but some studies have indicated that TB can increase with depth beyond a certain snow depth (Hofer & Mätzler, 1980; Mätzler et al., 1982; Schanda, 1983). Possible deviations in the snow scattering property from above theoretical factors are such as snow metamorphism, which dictates the internal structure of snow as it ages, and the multiple melt–freeze cycles, which together contribute to the complicated physical processes in the formation of snow structure; and snow redistribution that depends mainly on wind, terrain features, and land use (Armstrong, 1985; Hallikainen and Jolma, 1986; Rosenfeld & Grody, 2000; Rott & Nagler, 1995). In general, for areas below the treeline, snow is more variable spatially in an open environment than a protected environment such as a forest because in the former wind can more freely re-distribute the snow.

Volumetric scattering is a dominant loss mechanism for microwave radiation above 15 GHz for the case of dry snow. Therefore, TB retrieved from SSM/I sensor should reflect the dry snowpack properties such as the SWE. However, when snow becomes wet, which means increased dielectric constant, the information related to snowpack properties retrievable from SSM/I TB is reduced because in this case the absorption loss of microwave radiation dominates over scattering loss (Hallikainen, 1989). In addition to the effect of wet snow, Mätzler (1994) showed that the estimation of SWE by microwave radiometry is also hindered by varying grain size (depth-hoar), temperature gradient metamorphism, and the layering of snow pack within a sensor's footprint. Consequently, the effect of wet snow and depth-hoar should be removed from the SSM/I data before they can be used to estimate SWE reliably. Depth-hoar forms out of large temperature gradients between the warm ground and the cold snow surface, and it usually requires a thin snowpack combined with a clear sky or cold air temperature, and it often grows best at snow temperatures from -2°C to -15°C (Tremper, 2008).

Table 2

Physiographic and atmospheric data of Red River basin study area.

Data type	Source	Resolution/climate division
Land use classification	USGS	1 km
DEM	USGS	1 km
Precipitation (100 yrs) (Table 6)	State Climatology Office, Minnesota	5 climate divisions (CD) of North Dakota and 3 CD of Minnesota
Air temperature (Table 5) and snowfall (Fig. 2) for 30 climate stations	High Plains Climate Center, University of Nebraska	
Total precipitable water vapor (TPW)	TIROS Operational Vertical Sounder	1°

Conventional linear and nonlinear regression techniques have been widely used to retrieve SWE from remotely sensed data (e.g., Chang et al., 1996; Foster et al., 1997; Gan, 1996; Goodison & Walker, 1994; Hallikainen, 1989; Singh & Gan, 2000) possibly because of their simple structure. Given that TB is influenced by many snow parameters as discussed above, the TB–SWE relationship should be highly nonlinear. To our knowledge, artificial neural network (ANN) has not been used much for retrieving snow information from space platforms such as SSM/I, even though by its parallel computing structure that arises from neurons being interconnected by a network of three layers – input, hidden and output shown in Fig. 3, it probably holds more potential than regression models in estimating SWE. This leads to the motivation of this study with the primary objective of comparing the accuracy of SWE retrieved from SSM/I data of ascending and descending overpass time, physiographic and climate data by an ANN, with that retrieved by standard regressions models.

2. Study site and data description

The study site is the part of the Red River basin that lies between 100°W – 49°N and 95°W – 46°N , and is located in the eastern part of North Dakota and northwestern Minnesota (see Fig. 1). The catchment area of the site is approximately $120,000\text{ km}^2$ with the elevation ranging from 237 m to 552 m above mean sea level (AMSL). Its average annual precipitation is 520 mm. This study site, predominantly flat terrain with open farmland, was selected because of the large amount of good data available for model calibration and validation. The TB data from the SSM/I sensor, aboard the Defense Meteorological Satellite Program (DMSP) spacecraft, were taken from three different satellites, which are DMSP-F8 for 1988 and 1989 data, and DMSP-F10 and DMSP-F13 for the 1997 data (Table 1). The data used also included the airborne gamma-ray spectrometer data of NWS-USA (NWS, 1992) during the winter period of 1988, 1989, and 1997 (Table 1), which had a wide range of snowfall (Fig. 2). The physiographic and climate data used in the study are shown in Table 2. In this study, the 1989 SSM/I data that consist of both ascending and descending overpasses were first screened for wet snow and snow affected by depth-hoar, and then

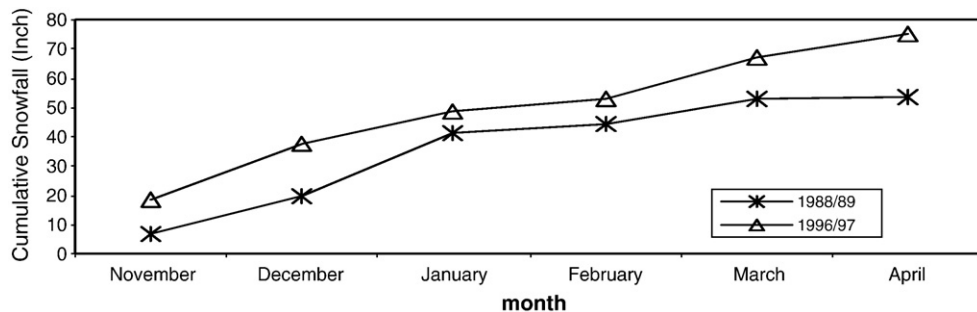


Fig. 2. Red River basin-wide mean cumulative snowfall at the end of each month during the study period.

combined to ensure sufficiently wide range of snow pack information for the calibration of the ANN model.

The retrieval of SWE from microwave data requires dry snow data in which volumetric scattering dominates over the absorption of microwave radiation from a snow pack. With increasing liquid water contents (wet snow), absorption starts to dominate over scattering as the major loss mechanism. In that case, the TB detected is independent of SWE (for wet snow) for the response is mostly from the topmost snow layer (Hallikainen, 1989). In this study, the SSM/I data (TB) affected by wet snow were screened by several dry snow criteria of Goodison et al. (1986) [$V37 < 250$ K and $(V19 - V37) \geq 9$ K], Goodison and Walker (1994) [$V37 - H37 \geq 10$ K], and one from NOAA-NASA SSM/I Pathfinder (NNSP) criteria ($V37 > 225$ K), which is based on the work of Neale et al. (1990).

For dry snow, besides SWE, the SSM/I TB also have strong dependence on the snow grain size (Chang et al., 1976), and this has prompted some researchers to use single grain size and single density in their models to simplify the SWE retrieval (Chen et al., 2001). Another important condition that influences microwave emission from snow is the extent of depth-hoar (large, loosely-bounded crystals) due to metamorphism at the base of the snow pack, which occurs when snow remains on the ground for a substantial portion of the winter and especially when air temperatures are very cold. Shallow snows are more susceptible of producing large grains of depth-hoar near the bottom because of higher temperature gradient in shallow than in deep snow packs (Zwally, 1977). Snowpack affected by depth-hoar could lead to over-estimation of SWE and so such data should be eliminated (Abdalati & Steffen, 1998). For deep snow packs, given an average seasonal surface temperature, it has been found that snow grain size profile increases with depth from top to bottom. For dry snow, the difference between the SSM/I TB of high frequency (37 GHz or 85 GHz) and low frequency channels (18 GHz or 19 GHz) of horizontal or vertical polarization provides information on SWE in a snow pack (e.g., Chang et al., 1982).

Chang et al. (1982) indicated the possibility of discriminating the effect of depth-hoar and the underlying ground condition (frozen or unfrozen) using the polarization factor, p -factor = $(V37 - H37) / (V37 + H37)$, e.g., the ratio of polarization difference and its sum. Singh and Gan (2000) used a p -factor > 0.026 to eliminate the SSM/I data that were affected by depth-hoar and the presence of water body of significant size in the vicinity of the footprint that has the effect of causing an underestimation of predicted SWE because of the high dielectric constant of the water body (underneath or presence of water in the snow pack due to above freezing temperature), which tends to reduce the overall TB due to high extinction loss (Hallikainen, 1989). However, the 1997 data were screened using a different p -factor (> 0.041) to account for the effect of data acquired from different spacecraft (DMSP F10 and F13), data type (Swath data) instead of DMSP F8 and EASE-Grid data for the 1988 and 1989 data. The presence of water bodies in a footprint was also modeled by including the area of water bodies, A_w , in Eq. (1).

3. Multivariate and projection pursuit regression models

Singh and Gan (2000) developed multivariate regression algorithms for retrieving SWE (Eqs. (1) and (2)) for the Red River basin which is predominantly open land with scattered vegetation and farmland. Given that the distribution of snow pack in Red River basin is greatly influenced by the winds because its open environment, the algorithms include parameters that reflect the physiographic and climate conditions, such as the AMSL, fraction of forest and water areas (A_f and A_w), total precipitable water (TPW), and air temperature (T_a).

$$SWE = K_1(V19 - H37) + K_2(AMSL) + K_3(1 - A_f) + K_4(1 - A_w)T_a + K_5TPW \quad (1)$$

$$SWE = K_6(TB.V19 - TB.V37) + K_7(TB.H19) + K_8(AMSL) + K_9A_f. \quad (2)$$

In Eq. (1), a nonlinear regression because it involves the product of two predictors A_w and T_a , was based on TB at 19 GHz and 37 GHz, AMSL, A_f , A_w , TPW, and T_a within the SSM/I footprint. While in Eq. (1), at-satellite TB, TPW, and T_a data were taken as separate variables, in Eq. (2), which is a linear regression, the surface/ground brightness temperature (T_{B_g}) was used instead. Given that electromagnetic waves are attenuated as they propagate through the atmospheric media, we expect the at-satellite TB to be smaller than T_{B_g} . We propose estimating T_{B_g} from the at-satellite TB by applying the atmospheric attenuation model (Choudhury, 1993), which uses T_a and TPW to address the effect of atmospheric water vapor on at-satellite TB given as

$$TB_{g,p} = (TB_{s,p} - T_{sky}) / t_a \quad (3)$$

$$t_a = \exp(-\tau / \mu) \quad (4)$$

$$\tau = 0.011 + 0.0026TPW \quad (\text{for } 19.3 \text{ GHz}) \quad (5)$$

$$\tau = 0.037 + 0.0021TPW \quad (\text{for } 37.0 \text{ GHz}) \quad (6)$$

$$T_{sky} = T_e(1 - t_a) \quad (7)$$

$$T_e = T_a - (8 + 0.06TPW) \quad (\text{for } 19.3 \text{ GHz}) \quad (8)$$

$$T_e = T_a - (18 + 0.12TPW) \quad (\text{for } 37.0 \text{ GHz}) \quad (9)$$

where the subscript p is the polarization (H or V), t_a is the atmospheric transmission coefficient, μ is the cosine of the incidence angle 53° (0.6 for SSM/I radiometer), TPW (in mm), τ is the optical thickness, T_{sky} is the sky temperature, T_e is the effective radiating temperature (isothermal air temperature), T_a is the air temperature, $T_{B_{s,p}}$ is the at-satellite TB, and $T_{B_{g,p}}$ is the surface/ground TB.

For the Red River Basin, introducing such terms account for the effects of AMSL, forest cover and water bodies on the TB captured by the SSM/I sensor, but it could erroneously give a value of SWE in case of no snow. Therefore Eqs. (1) and (2) should be applied mainly to the November–April period during which snowpack should be expected at the Red River Basin, and the estimated SWE should be cross examined with ground measurements if available. It is also possible to find out the snowfall conditions of a river basin using data from the western United States Snow Telemetry (SNOTEL) network of snow pressure pillows.

Singh and Gan (2000) also estimated the SWE (predictand) from SSM/I TB data, physiographic and atmospheric data (predictors) using the non-parametric, Projection Pursuit Regression (PPR) of Friedman and Stuetzle (1981). PPR models the response variable as a sum of functions of linear combinations of predictor variables. Suppose y and x 's denote response and predictor vectors respectively, PPR finds the number of terms M_0 , direction vectors ($\alpha_1, \alpha_2, \dots, \alpha_{M_0}$) and nonlinear transformations ($\phi_1, \phi_2, \dots, \phi_{M_0}$) as shown in Eq. (10),

$$\hat{y} \approx \bar{y} + \sum_{m=1}^{M_0} \beta_m \phi_m(\alpha_m^T x). \quad (10)$$

Through minimizing the expected distance or mean square error between y (e.g., observed SWE) and \hat{y} (estimated SWE) using Eq. (11), the model parameters β_m (the response linear combinations), α_m (the direction vectors), ϕ_m (the predictor functions), for $m = 1, 2, \dots, M_0$ are obtained.

$$L_2(\beta, \alpha, \phi, x, y) = E[y - \hat{y}]^2. \quad (11)$$

The use of PPR lies in selecting an optimum number of terms, M_0 , determined by trial and error, often by starting the algorithm with a large M_0 and then decreasing M_0 such that the increase in accuracy due to an additional term is not worth the increased complexity (Friedman, 1985). The optimum M_0 is determined in terms of the

fraction of variance it cannot explain (Friedman & Stuetzle, 1981; Morton, 1989). From Eq. (11), this unexplained variance, U is given as

$$U = \frac{L_2(\beta, \alpha, \phi, x, y)}{\text{Var}(y)} \quad (12)$$

4. Artificial neural network (ANN) model

ANN models have been widely used in many fields of research (e.g., Clair & Ehrman, 1998; Davis et al., 1993; Foody, 1999; Saad et al., 1994; Smith & Eli, 1995; Tedesco et al., 2004; Thirumalaiah & Deo, 1998) because of their capability of modeling nonlinear and poorly understood systems (Ward & Redfern, 1999). The power of ANN is partly associated with their inherent non-linearity and complex internal structure that resembles the human brain in acquiring and storing knowledge through a learning process (Haykin, 1994). During the training process, the acquired knowledge is stored in the connection weights joining the one input, one or more hidden, and one output layers (only one hidden layer is shown in Fig. 3). The strength of connections depends on the connection weights. The input to each neuron in the next layer is the sum of all its incoming connection weights multiplied by their respective neuron values adjusted with an offset, and the result is fed into activation function of the neuron, which can be the non-linear sigmoid function, the simple linear activation, threshold activation, or the hyperbolic tangent. Other than some drawbacks such as being classified as black box models, the problem of over-fitting and tedious training, ANN can approximate almost any function (Tsukimoto, 2000).

Among the widely used ANN models is the multi-layer feed forward neural network (MFNN), but its training process is very time consuming because of its model structure (Gupta et al., 1997). On the other hand, the less popular Modified Counter Propagation Network (MCPN) has shown to be superior (Hsu et al., 1999) because its structure makes the training process easier. Moreover, it produces intermediate results that can be analyzed if needed. The MCPN makes use of the self-organizing feature map (SOFM) learning algorithm of Kohonen (1989) that has many successful applications (Kohonen et al., 1996) because of its model structure and learning ability (Lu & Basar, 1998). On the basis of its past success, MCPN was selected as the ANN for this study. MCPN consists of an interconnected network of three layers, namely, the input, hidden, and output layers (Fig. 3). The un-supervised clustering procedure of SOFM performs the input-hidden layer transformation ($SD_i \rightarrow IP_j$). This constitutes the non-linear part of the input/output mapping. The training of SOFM is carried out by computing, for each hidden node, the distance d_j between the normalized input vector (SD_i which is the input snow data given in Table 3) and the weighting vector w_{ji} as

$$d_j = \sqrt{\sum_{i=1}^{n_0} (SD_i - w_{ji})^2} \quad j = 1, \dots, n_1 \quad (13)$$

where n_0 is the number of input variables (6 or 4), and n_1 is the number of hidden nodes. Among the competing hidden nodes, c is the

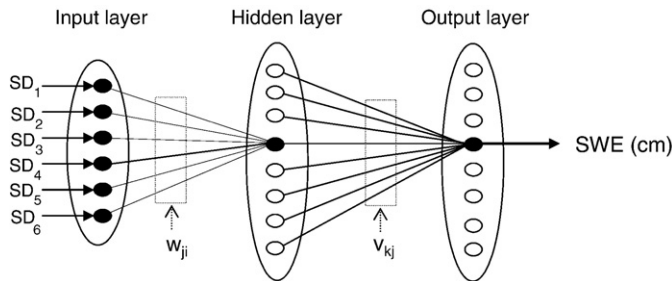


Fig. 3. The Modified Counter Propagation Network (MCPN) architecture indicating the possible input variables (SD_i) with the corresponding output (SWE), and the connection weights w_{ji} and v_{kj} .

Table 3
Input parameters of the ANN (MCPN) model for both cases 1 and 2.

SD_i	1	2	3	4	5	6
Case 1	V19 – H37	AMSL	1 – A_F	1 – A_W	T_a	TPW
Case 2	TB _g V19 – TB _g V37	TB _g H19	AMSL	A_F		

winning node such that the distance d_j is the smallest ($d_c = \min(d_j), j = I_c$). To complete the SOFM training, the updating of weights w_{ji} is performed only for the hidden nodes in the neighborhood Λ_c surrounding the winner node as

$$w_{ji}(t) = w_{ji}(t - 1) + \eta(t)(SD_i - w_{ji}(t - 1)), \text{ for } j \in \Lambda_c(t) \quad i = 1, 2, \dots, n_0, 0 < \eta(t) < 1$$

$$w_{ji}(t) = w_{ji}(t - 1) \quad \text{Otherwise} \quad (14)$$

with t being the iteration counter for the training process, and $\eta(t)$ is the learning rate which together with $\Lambda_c(t)$ are decreased after each iteration from their initial settings of $\eta_0 = 0.2-0.5$ and $\Lambda_0 = n_1 / 2$ (Hsu et al., 1999). Herein, a stopping criterion of 2000 iterations was used to optimize w_{ji} , or when a fixed goodness-of-fit criterion ($R^2, E_f, RMSE$, or bias) is reached. The accuracy of the approximation depends mainly on training data. Before performing the hidden–output layer transformation, the intermediate output parameters, IP_j , corresponding to the input vector, SD_i , are computed as

$$IP_j = 1 - d_j \quad \text{for } j \in \Omega$$

$$IP_j = 0 \quad \text{otherwise} \quad (15)$$

where Ω is the size of hidden nodes centered on the neighborhood of I_c . As the dimension of Ω should be equal to or greater than that of the input vector, a size of 8×8 was selected in this study.

The training of the weights, v_{kj} , required for the hidden–output transformation ($IP_j \rightarrow SWE_k$), is performed by a supervised process based on a simple recursive gradient search of the Local Linear Output Mapping (LLOM). The linear least square estimation, which is a batch training procedure, is used to obtain the initial estimates of v_{kj} based on the input–output data set. For nodes in the neighborhood of Ω surrounding the active node, a sequential training algorithm is used to recursively update these weights as

$$v_{kj}(t) = v_{kj}(t - 1) + \beta(T_{SWE_k} - SWE_k)_{y_j}, \text{ for } j \in \Omega, k = c \quad (16)$$

where β is the learning step size ($0 \leq \beta \leq 1$), and T_{SWE_k} is the observed (target) SWE and SWE_k is its estimated value after each iteration. Through this process, adjustments are made to v_{kj} to obtain their final values, where 100 iterations and a β value of 0.1 were used in this study. Thereafter, the final adjusted v_{kj} together with IP_j are used to compute the model output, SWE_k according to

$$SWE_k = \sum_j v_{kj} IP_j \quad \text{for } j \in \Omega, k = c$$

$$SWE_k = \emptyset \quad \text{for } k \neq c \quad (17)$$

To train the network over a wide range of values, a wet (1997) and a dry year (1989) data were used. To ensure no over-fitting, the calibrated network is validated with another data set not used in the calibration.

5. Discussions of results

The performance of a model depends on factors such as model structure, calibration procedure, information content of the input data and its associated data processing. The ANN (MCPN) results were compared to the nonlinear regression (Eq. (1)) and PPR algorithms (Eq. (10)). Due to insufficient data in 1988, the second algorithm (Eq. (2)) calibrated with the 1988 data by Singh and Gan (2000) was not compared.

The ANN model (MCPN) was calibrated from SSM/I TB, physiographic and climate data of 1989 and then validated by the 1997 data. An ANN with a large number of nodes will give rise to many parameters which could be difficult to train (excessive training time and possibly over-fitting) if the amount of data available for model calibration is relatively short. On the other hand, an ANN with small number of nodes can learn only few interactions, while the one with many nodes can learn more (Hsieh & Tang, 1998). As a trade off, we have kept the number of hidden (SOFM) nodes as 8 because it has to be equal or greater than input nodes, which were 6 and 4 for cases 1 and 2, respectively.

In developing the ANN model, the SSM/I data were screened for effects of wet snow, depth-hoar and presence of water body through the criteria of Goodison et al. (1986), Walker and Goodison (1993), and the p -factor (>0.026 or >0.041 depending on the satellite used) as described in Section 2. No separation was made between ascending and descending portion of the 1997 data of DMSP-F10 and F13 partly to make use of all available data to validate the ANN model, partly because all the data (ascending and descending) contains information on SWE, and the results obtained for both the calibration and validation stages are close to each other, a sound basis for accepting the validity of the calibrated ANN model, as explained below.

The performance of ANN based on the input parameters for cases 1 and 2 (with reference to Eqs. (1) and (2) respectively, and Table 3) was assessed by the coefficient of determination (R^2), correlation coefficient (ρ), Nash Sutcliffe coefficient (E_f) (Nash & Sutcliffe, 1970), root mean square errors (RMSE), and Bias. Compared to the nonlinear regression that requires a shift parameter (SP) in the validation stage to get good results because of different scattering albedo between snowpacks of calibration and validation stages (see more detailed explanations in Singh & Gan, 2000), ANN results were relatively better in both calibration (R^2 of 0.894 against 0.778) and validation (R^2 of 0.916 over 0.708) stages (Table 6). Although no shift parameter was used in the validation stage, MCPN was able to produce more reliable results than the nonlinear regression (Eq. (1)) using less input data because to get an appropriate shift parameter, a sample average of SWE for that particular period was needed. The superior results of MCPN compared to the nonlinear regression (Eq. (1)), can be partly attributed to the inherent non-linearity and inter-connectivity of the ANN structure, together with its ability to learn and generalize information from complex systems as opposed to the simple input/output model structure of the nonlinear regression model.

The calibration results for MCPN and PPR (Eq. (10)) were more or less similar, but in both cases 1 and 2 MCPN did better than PPR in the validation stage, even though PPR also needed a shift parameter at the validation stage as nonlinear regression (Table 6). Given that PPR did better than the regression model, this further demonstrates that between regression, PPR and MCPN (ANN), MCPN gave the best results in Red River Basin, then PPR and finally the regression algorithm.

While Foster et al. (1997) indicated that horizontal polarization is more sensitive than vertical polarization in vegetated areas, Goodison and Walker (1994) proposed an algorithm using vertically polarized brightness temperature difference (V19 – V37), which provided very consistent and compatible SWE over the Canadian prairies. Given that the Red River basin has a prairie-like environment with some few scattered vegetation, Case 1 used a mixture of vertical and horizontal

Table 5
Red River basin mean monthly and annual precipitation (cm).

Year/month	Oct	Nov	Dec	Jan	Feb	Mar	Apr	Annual
100 years (normal)	3.72	2.02	1.47	1.47	1.33	2.30	4.12	52.07
1988/89	1.07	2.72	2.24	3.00	0.69	3.68	3.10	45.21
1996/97	5.82	4.50	2.72	3.53	0.97	3.23	5.99	56.64

polarization (V19 and H37), while the effects of forest cover and water bodies were removed by $(1 - A_f)$ and $(1 - A_w)$, and the effects of terrain and climate were accounted for via AMSL, T_a , and TPW, respectively. Case 2 (based on Eq. (2)) was formulated to test the advantage of using surface/ground brightness temperature (T_{B_g}) derived from the at-satellite TB and the atmospheric effect accounted for by the atmospheric attenuation model of Choudhury (1993) (Eqs. (3)–(9)), and the vegetation cover effect considered in last the term of Eq. (2). The effect of the water body was indirectly considered by screening off affected data using the p -factor (>0.026 or >0.041 depending on the satellite data used).

It can be seen (Table 6) that, Case 1 performed slightly better than Case 2 in the Calibration stage in terms of all test statistics (e.g., E_f of 0.800 over 0.762). This may be partly attributed to Case 1 explicitly considering the effect of water body in the SSM/I footprint by the term $(1 - A_w)$, instead of data screening by the p -factor adopted in Case 2. Also, there were possibly errors associated with the atmospheric attenuation model (Eqs. (3)–(9)) used to convert the at-satellite TB to surface/ground brightness temperature (T_{B_g}) in Case 2, partly because of model assumptions and model parameters used in say, Eqs. (5), (6), (8) and (9), and partly because of data errors such as TPW retrieved from the operational vertical sounder of the TIROS (Television and Infrared Observation Satellite) satellite. Chen et al. (1996) found that TPW and topospheric humidity of two sensors (SSM/I and TIROS-N) agreed with the vapor distribution simulated by the ECHAM-4 general circulation model in terms of mean, seasonal and inter-annual variations but there are biases in details. The effect of atmospheric attenuation in the Prairies during winter was likely not significant as the (total precipitable water) TPW was relatively small and of coarse resolution (1° latitude by 1° longitude) as compared to TB data ($25 \text{ km} \times 25 \text{ km}$ pixels). Given that differences between TB and T_{B_g} were small, the gain obtained from converting TB to T_{B_g} may be marginal. In the validation stage, Table 6 shows that, although the performance between Cases 1 and 2 was almost similar (e.g., E_f of 0.838 against 0.855), Case 2 performed slightly better than Case 1 in all test statistics. This can be attributed to using validation data (1997 data) that are different from calibration data in terms spacecraft (F10 and F13 versus F8), snowpacks exposed to a different metamorphism process (due to different air temperature (see Table 4), wind speed and direction, the 1988/89 was a relatively dry year while 1996/97 a relatively wet year (see Table 5 and Fig. 2), and length of time that snow was on the ground) from their calibration counterparts (1989 data).

In both cases 1 and 2, the calibration result of the ANN model was slightly poorer than the validation counterpart (see Table 6) which is surprising, e.g., Case 1 (E_f of 0.800 over 0.838) and Case 2 (E_f of 0.762 against 0.855). This is partly because the amount of snowfall was higher in 1997 than in 1989 (see Fig. 2), e.g., the SWE in 1997 (mean

Table 4
Weekly maximum and minimum air temperature ($^\circ\text{C}$) of the Red River basin corresponding to the 1989 and 1997 Airborne SWE data collection.

Year	Month	February				March				April		
		1	2	3	4	1	2	3	4	1	2	3
1989	Min	-28.3	-17.6	-26.0	-18.7	-23.5	-5.5	-19.2	-5.3	-3.4		
	Max	-19.0	-5.2	-13.5	-6.4	-11.7	1.5	-5.9	2.3	6.0		
1997	Min	-14.9	-21.4	-16.4	-18.5	-20.0	-15.8	-14.3	-4.2	-4.9	-10.7	-1.7
	Max	-4.6	-7.5	-3.1	-5.3	-7.6	-4.4	-1.5	4.6	3.8	-0.5	10.2

Table 6

Calibration and validation results of the nonlinear regression (Eq. (1)), projection pursuit regression (Eq. (10)), and artificial neural network (MCPN) cases 1 and 2.

	Data	Mode	R^2	E_f	RMSE ^a (%)	Bias ^a (%)	SP
Eq. (1)	1989	C	0.778	0.696	121.1	0.34	0.00
	1997	V	0.708	0.634	346.7	0.96	+4.00
Eq. (10)	1989	C	0.857	0.760	73.5	0.20	0.00
	1997	V	0.623	0.557	442.8	1.23	+4.00
Case 1	1989	C	0.894	0.800	10.5	0.03	–
	1997	V	0.916	0.838	8.97	–0.01	–
Case 2	1989	C	0.873	0.762	11.76	–0.01	–
	1997	V	0.923	0.855	8.485	–0.0044	–

C = calibration; V = validation; R^2 = coefficient of determination; E_f = Nash and Sutcliffe (1970) coefficient; RMSE = root mean square error; and SP = shift parameter (cm).

^a See Appendix A for equations of RMSE (%) and Bias (%).

SWE = 13.50 cm) was higher than that of 1989 (mean SWE = 9.24 cm) (Table 1). Table 4 shows that the weekly maximum air temperatures for February and March were much cooler and more highly variable for 1989 (–19 °C to 2.3 °C) than for 1997 (–7.6 °C to 4.6 °C). Because relatively large snowfall occurred in 1997 compared to 1989, the effect of depth-hoar should more pronounced in the shallow snowpack of 1989 than the deep snowpack of 1997. So, even though generally MCPN

parameters were well calibrated (a sufficient and good quality data set is always essential to achieve a good calibration by activating all the model parameters during the calibration stage), the better validation results may partly indicate that validation data of 1997 were of better quality than calibration data of 1989. The difference in data sources (DMSP F10 and F13 instead of DMSP-F8; Swath data instead of EASE-Grid data) between 1997 and 1989 may have also contributed to better validation than calibration results. However, the good validation results at least indicate that MCPN was properly calibrated.

Besides the above statistics, the performance of MCPN was also assessed with respect to SWE observed from airborne gamma data by scatterplots (see Fig. 4). In both cases 1 and 2, likely for reasons explained above, the scatters is relatively larger in the calibration than in the validation stages. In addition, there were more underestimations of predicted SWE in Case 2 than in Case 1 because water bodies were not explicitly considered in Case 2 which could lead to some reduction in the brightness temperature because of high extinction loss. There were six airborne flight lines of 1989 and 1997 that fell in three SSM/I footprints, of which 12.7%, 6.1%, and 4% of footprint areas respectively were covered by water bodies. However, this problem of water body effect on TB (e.g., higher underestimation of large SWE for Case 2 than Case 1 in the calibration stage, see Fig. 4, was probably partly corrected by screening the data for Case 2 using the p -factor (>0.026 or >0.041).

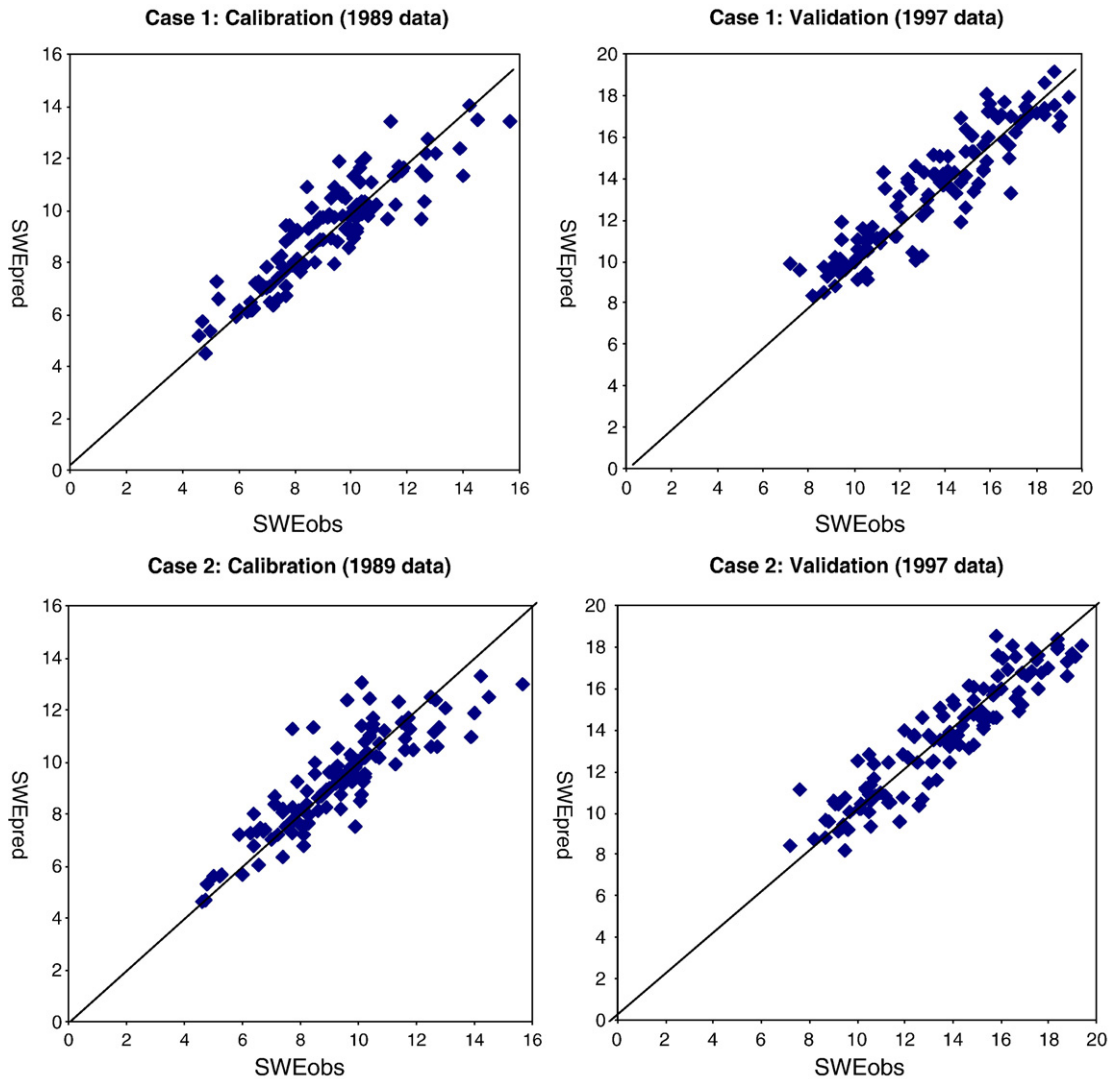


Fig. 4. Scatter plots of observed (x-axis) versus predicted (y-axis) snow water equivalent (SWE) for Red River basin under both calibration and validation stages using the artificial neural network (MCPN) model.

6. Summary and conclusions

On the basis of airborne gamma-ray measurements collected through the Radiation Survey Program of NWS-USA as the observed snow water equivalent (SWE), the MCPN (an artificial neural network model) was trained against two cases of input nodes, respectively set up using at-satellite, SSM/I brightness temperature (TB) of DMSP-F8, and surface/ground brightness temperature (TB_g) data derived from at-satellite TB, to simulate the 1989 SWE for the Red River Basin of North Dakota and northwestern Minnesota. The SSM/I data, of 19 and 37 GHz frequencies and in both horizontal and vertical polarization, were screened to eliminate footprints affected by wet snow, large water bodies and depth-hoar. The input data also included physiographic and climate data. Then driving the calibrated MCPN with SSM/I data taken from DMSP-F10 and DMSP-F13 satellites for 1997, the simulated SWE was validated against the corresponding observed 1997 SWE data.

The MCPN model results obtained were better than those of a PPR, which in turn was better than that of multivariate nonlinear regression, in both calibration and validation stages (see Table 6). It seems that MCPN is more versatile and powerful than PPR and nonlinear regression models in retrieving SWE from passive microwave data of SSM/I because of its parallel computing structure that arises from neurons being interconnected by a network, and complex internal structure that makes them capable of learning complex input–output mappings without a direct knowledge of the underlying physical processes of the system. Tedesco et al. (2004) also found ANN to perform better than other algorithms in mapping the SWE of Finland. Lastly, as previously shown by others (e.g., Armstrong & Brodzik, 2002), the results demonstrate the feasibility of retrieving regional SWE data from passive microwave data of SSM/I.

Lastly, the freeze and thaw cycle gives rise to re-frozen ice layers in snow pack, or large-scale cyclones can transfer sufficient energy to increase the air temperature close to melting point, and such melt-layers can re-freeze, which could affect the retrieval of SWE from passive microwave data, and which should be a focus of future research in retrieving SWE from such data.

Acknowledgements

This project was partly funded by the NSERC of Canada. The second and third authors were also supported by the University of Alberta Ph.D. Scholarship, and teaching assistantship. Dr. T. Carroll of the Airborne Gamma Radiation Survey Program (k0) of NWS-USA provided the gamma-ray spectrometer SWE data.

Appendix A

Root mean square error

$$\text{RMSE}(\%) = \sqrt{\frac{\sum_{i=1}^n (\text{SWE}_{\text{SSM/I}} - \text{SWE}_{\text{Obs}})^2}{n}} * \frac{100}{\text{Mean}_{\text{SWE}_{\text{Obs}}} - \text{SWE}_{\text{Obs}}}$$

$$\text{Bias}(\%) = \frac{\sum_{i=1}^n (\text{SWE}_{\text{SSM/I}} - \text{SWE}_{\text{Obs}})}{\sum \text{SWE}_{\text{Obs}}} * 100.$$

References

Abdalati, W., & Steffen, K. (1998). Accumulation and hoar effects on microwave emission in Greenland and ice-sheet dry-snow zones. *Journal of Glaciology*, 44 (148), 523–531.

Armstrong, R., 1985. Metamorphism in a subfreezing seasonal snow cover, Ph.D. thesis, University of Colorado, Boulder.

Armstrong, R., & Brodzik, M. J. (2002). Hemispheric-scale comparison and evaluation of passive microwave snow algorithms. *Annals of Glaciology*, 34, 38–44.

Armstrong, R., Brodzik, M.J., Savoie, M.H., 2003. Snow cover validation. National Snow and Ice Data Center (NSIDC), AMSR-E Joint Science Team Meeting, Monterey CA, October 21–22. (<http://weather.msfc.nasa.gov/AMSR/>).

Chang, A., Foster, J. L., & Hall, D. K. (1996). Effects of forest on the snow parameters derived from microwave measurements during the boreal. *Hydrological Procedure*, 10, 1565–1574.

Chang, A. T. C., Foster, J. L., Hall, D. K., Rango, A., & Hartline, B. K. (1982). Snow water equivalent accumulation by microwave radiometry. *Cold Regions Science and Technology*, 5(3), 259–267.

Chang, A. T. C., Gloersen, P., Schmugge, T., Wilheit, T. T., & Jwally, H. J. (1976). Microwave emission from snow and glacier ice. *Journal of Glaciology*, 16(74), 23–39.

Chen, C.-T., Nijssen, B., Guo, J., Tsang, L., Wood, A. W., Hwang, J.-N., et al. (2001). Passive microwave remote sensing of snow constrained by hydrological simulations. *IEEE Transactions on Geoscience and Remote Sensing*, 39(8), 1744–1756.

Chen, C.-T., Roekner, Erich, & Soden, Brian J. (1996). A comparison of satellite observations and model simulations of column-integrated moisture and upper-tropospheric humidity. *Journal of Climate*, 9(7), 1561–1585.

Choudhury, B. J. (1993). Reflectivities of selected land surfaces types at 19 and 37 GHz from SSM/I observations. *Remote Sensing of Environment*, 46, 1–17.

Clair, T. A., & Ehrman, J. M. (1998). Using neural networks to assess the influence of changing seasonal climates in modifying discharge, dissolved organic carbon, and nitrogen export in eastern Canadian rivers. *Water Resources Research*, 34(3), 447–455.

Davis, D. T., Chen, Z., Tsang, L., Hwang, J. N., & Chang, A. T. C. (1993). Retrieval of snow parameters by iterative inversion of a neural network. *IEEE Transactions on Geoscience and Remote Sensing*, 31, 842–851.

Dyer, J. L., & Mote, T. L. (2007). Trends in snow ablation over North America. *International Journal of Climatology*, 27, 739–748. doi:10.1002/joc.1426

Ferraro, R., Grody, N., Forsyth, D., Carey, R., Basist, A., Janowiak, J., et al. (1994). Microwave measurements produce global climatic, hydrologic data. *EOS Transactions, AGU*, 75(30), 337–343.

Foody, G. M. (1999). The significance of border training patterns in classification by a feed forward neural network using back propagation learning. *International Journal of Remote Sensing*, 20(18), 3549–3562.

Foster, J. L., Chang, A. T. C., & Hall, D. K. (1997). Comparison of snow mass estimates from a prototype passive microwave snow algorithm, a revised algorithm and snow depth climatology. *Remote Sensing Environment*, 62, 132–142.

Friedman, J. H. (1985). Classification and multiple regression through projection pursuit. *Technical Report LCS012*: Department of Statistics, Stanford University.

Friedman, J. H., & Stuetzle, W. (1981). Projection pursuit regression. *Journal of the American Statistical Association*, 82, 249–266.

Gan, T. Y. (1996). Passive microwave snow research in Canadian high arctic. *Canadian Journal of Remote Sensing*, 22(1), 36–44.

Goodison, B. E. (1989). Determination of areal snow water equivalent on Canadian prairies using passive microwave satellite data. In *Proc. IEEE Int. Geoscience and Remote Sensing, Symp.'89, Vol. 3*. (pp. 243–246) Vancouver, BC, Canada.

Goodison, B. E., Rubinstein, I., Thirkettle, F. W., & Langham, E. J. (1986). *Determination of snow water equivalent on the Canadian prairies using microwave radiometry, Vol. No. 155*. (pp. 163–173): IAHS Publ.

Goodison, B. E., & Walker, A. E. (1994). Canadian development and use of snow cover information from passive microwave satellite data. *ESA/NASA International Workshop* (pp. 245–262).

Gupta, H. V., Hsu, K., & Sorooshian, S. (1997). Superior training of artificial neural networks using weighted-space partitioning, paper presented at 1997. *IEEE Int. Conf. on Neural Networks Houston, Tex*: Inst. of Electr. and Electron. Eng.

Hall, D. K., Riggs, G. A., Salomonson, V. V., DiGirolamo, N. E., & Bayr, K. A. (2002). MODIS snow-cover products. *Remote Sensing of Environment*, 83, 181–194.

Hallikainen, M. T. (1989). Microwave radiometry on snow. *Advanced Space Research*, 9(1), 267–275.

Hallikainen, M., & Jolma, P. (1986). Retrieval of water equivalent in Finland by satellite microwave radiometry. *IEEE Transactions on Geoscience and Remote Sensing*, GE-24, 855–862.

Hallikainen, M. T., & Jolma, P. A. (1992). Comparison of algorithms for retrieval of snow water equivalent from Nimbus-7 SMMR data in Finland. *IEEE Transactions on Geoscience and Remote Sensing*, 30, 124–131.

Haykin, S. (1994). *Neural networks: A comprehensive foundation*. New York: MacMillan.

Hofer, R., & Mätzler, C. (1980). Investigation of snow perimeters using microwave radiometry in the 3- to 60-mm wavelength region. *Journal of Geophysical Research*, 85(C1), 453–460.

Hsieh, W. W., & Tang, B. (1998). Applying neural network models to prediction and data analysis in meteorology and oceanography. *Bulletin of the American Meteorological Society*, AMS, 79(9), 1855–1870.

Hsu, K., Gupta, H. V., Gao, X., & Sorooshian, S. (1999). Estimation of physical variables from multi-channel remotely sensed imagery using a neural network: Application to rainfall estimation. *Water Resources Research*, 35(5), 1605–1618.

Kohonen, T. (1989). *Self-organization and associative memory*, 3rd ed. New York: Springer-Verlag.

Kohonen, T., Oja, E., Simula, O., & Kangas, J. (1996). Engineering application of the self-organizing map. *Proc. IEEE*, 84(10), 1358–1383.

Lu, S., & Basar, T. (1998). Robust nonlinear systems identification using neural networks models. *IEEE Transactions on Neural Networks*, 9(3).

Mätzler, C. (1994). Passive microwave signatures of landscapes in winter. *Meteorology and Atmospheric Physics*, 54, 241–260.

Mätzler, C., Schanda, E., & Wood, W. (1982). *Toward the definition of optimum sensor specifications for microwave remote sensing of snow* IEEE Trans. Geosci. Remote Sensing, Vol. GE-20. (pp. 57–66).

- Mekis, ., & Hopkinson, R. (2004). Derivation of an improved snow water equivalent adjustment factor map for application on snowfall ruler measurements in Canada. *Proceedings, Fourteenth Conference on Climatology, Seattle, WA* (pp. 12–15).
- Morton, S.C., 1989. *Interpretable projection pursuit*, Ph.D. thesis, Stanford University, 109p.
- Nash, J. E., & Sutcliffe, J. V. (1970). River flow forecasting through conceptual models; Part 1 – A discussion of principles. *Journal of Hydrology*, 10(3), 282–290.
- Neale, C. M. U., McFarland, M. L., & Chang, K. (1990). Land-surface-type classification using microwave brightness temperatures from the special sensor microwave/imager. *IEEE Transactions on Geoscience and Remote Sensing*, 28(5), 829–837.
- NWS (1992). Airborne gamma radiation snow survey program and satellite hydrology program: User's guide. *Office of Hydrology, National Weather Service, NOAA, US Department of Commerce, Minnesota* 54pp.
- Rosenfeld, S., & Grody, N. C. (2000). Metamorphic signature of snow revealed in SSM/I measurement. *IEEE Transactions on Geoscience and Remote Sensing*, 38(1), 53–63.
- Rott, H., & Nagler, T. (1995). Intercomparison of snow retrieval algorithms by means of spaceborne microwave radiometry. In B. J. Choudhury, Y. H. Kerr, E. G. Njoki, & P. Pampaloni (Eds.), *Passive microwave remote sensing of Land-Atmosphere Interactions* (pp. 227–241). Utrecht, The Netherlands: VSP.
- Saad, M., Turgeon, A., Bigras, P., & Duquette, R. (1994). Learning disaggregation technique for the operation of long-term hydrologic power system. *Water Resources Research*, 30(11), 1395–3202.
- Salomonson, V. V., & Appel, I. (2006). Development of the Aqua MODIS NDSI fractional snow cover algorithm and validation results. *IEEE Transactions on Geoscience and Remote Sensing*, 44(7), 1747–1756.
- Schanda, E. (1983). Selection of microwave bands for global detection of snow. *Advances in Space Research*, 3(2), 303–308.
- Shi, J., & Dozier, J. (2000). Estimation of snow water equivalent using SIR-C/X-SAR, Part I: Inferring snow density and subsurface properties. *IEEE Transactions on Geoscience and Remote Sensing*, 38(6), 2465–2474.
- Singh, P. R., & Gan, T. Y. (2000). Retrieval of snow water equivalent using passive microwave brightness temperature data. *Remote Sensing of Environment*, 74, 275–286.
- Smith, J., & Eli, R. N. (1995). Neural network model of rainfall–runoff process. *ASCE Journal of Water Resources Planning and Management*, 121(6), 449–508.
- Sobolowski, S., & Frei, A. (2007). Lagged relationships between North American snow mass and atmospheric teleconnection indices. *International Journal of Climatology*, 27, 221–231. doi:10.1002/joc.1395
- Tedesco, M., Pulliainen, J., Takalab, M., Hallikainen, M., & Pampaloni, P. (2004). Artificial neural network-based techniques for the retrieval of SWE and snow depth from SSM/I data. *Remote Sensing of Environment*, 90, 76–85.
- Tekeli, E., Akyurek, A., Sensoy, A., & Sorman, A. U. (2005). Using MODIS snow cover maps in modeling snowmelt runoff process in the eastern part of Turkey. *Remote Sensing of Environment*, 97, 216–230.
- Tremper, B. (2008). *Staying Alive in Mountainous Terrain*, 2nd ed. *The Mountaineers Books* (304 pp.).
- Thirumalaiah, K., & Deo, M. C. (1998). River stage forecasting using artificial neural networks. *ASCE Journal of Hydrologic Engineering*, 4(3), 232–239.
- Tsang, L., Chen, C. T., Chang, A. T. C., Guo, J., & Ding, K. H. (2000). Dense media radiative transfer theory based on quasicrystalline approximation with applications to passive microwave remote sensing of snow. *Radio Science*, 35(3), 731–749.
- Tsukimoto, H. (2000). Extracting rules from trained neural networks. *IEEE Transactions on Neural Networks*, 11(2).
- Walker, A. E., & Goodison, B. E. (1993). Discrimination of a wet snow cover using passive microwave satellite data. *Annals of Glaciology*, 17, 307–311.
- Ward, B., & Redfern, S. (1999). A neural network model for predicting the bulk-skin temperature difference at the sea surface. *International Journal of Remote Sensing*, 20(18), 3533–3548.
- Wilson, L., Tsang, L., Hwang, J.-N., & Chen, C.-T. (1999). Mapping snow water equivalent in the mountainous areas by combining a spatially distributed snow hydrology model with passive microwave remote sensing data. *IEEE Transactions on Geoscience and Remote Sensing*, 37, 690–704.
- Zwally, H. J. (1977). Microwave emissivity and accumulation rate of polar firn. *Journal of Glaciology*, 18, 195–215.